Structure and Thermodynamics of Eu(III) and Cm(III) Complexes with Glucuronic Acid

Reese, S.; Kaden, P.; Taylor, C. J.; Kloditz, R.; Schmidt, M.;

Originally published:

September 2021

Inorganic Chemistry 60(2021)19, 14667-14678

DOI: https://doi.org/10.1021/acs.inorgchem.1c01746

Perma-Link to Publication Repository of HZDR:

https://www.hzdr.de/publications/Publ-33241

Structure and Thermodynamics of Eu(III) and Cm(III) Complexes with Glucuronic Acid

Sebastian Reese,[a,†] Peter Kaden,[a] Corey J. Taylor,[a] Roger Kloditz[a] and Moritz Schmidt[a,*]

[a)] Helmholtz-Zentrum Dresden – Rossendorf, Institute of Resource Ecology, Bautzner Landstr. 400, 01328 Dresden, Germany.
† Current address: ROTOP Pharmaka GmbH, Bautzner Landstraße 400, 01328 Dresden, Germany.
*Corresponding author: moritz.schmidt@hzdr.de, +49 351 260 3156

Abstract

Complexation by small organic ligands controls the bioavailability of contaminants and influences their mobility in the geosphere. We have studied the interaction of Cm^{3+} as a representative of the trivalent actinides and Eu^{3+} as an inactive homologue with glucuronic acid (GlcA) a simple sugar acid. Time-resolved laser-induced luminescence spectroscopy (TRLFS) shows that complexation at pH = 5.0 occurs only at high ligand-to-metal ratios in the form of 1:1 complexes with standard formation constants $log\beta^0$ = 1.84 ± 0.22 for Eu^{3+} and $log\beta^0$ = 2.39 ± 0.19 for Cm^{3+}. A combination of NMR, QMMM, and TRLFS reveals the structure of the complex to be a "half-sandwich-structure" wherein the ligand binds through its carboxylic group, the ring oxygen, and a hydroxyl group in addition to five to six water molecules. Surprisingly, Y^{3+}, which was used as a diamagnetic reference in NMR, prefers a different coordination geometry with bonding through at least two hydroxyl groups on the opposite side of a distorted GlcA molecule. QMMM simulations indicate that the differences in stability between Cm, Eu, and Y are related to ring strain induced by smaller cations. At higher pH a stronger complex was detected, most likely due to deprotonation of a coordinating OH-group.

1 Introduction

The actinides (An) are a group of radioactive heavy elements, some of which are highly radiotoxic. This is of concern for instance with respect to the final disposal of nuclear waste,[1, 2] as well as for the remediation of so-called legacy sites.[3, 4] The transuranic elements Pu and Am are a particular problem, due to their long half-lives ($t_{1/2}(^{239}Pu)$ = 24,100 a; $t_{1/2}(^{243}Am)$ = 7430 a), which means they will remain highly toxic over long periods of time.[2] Pu is stable in a number of oxidation states from III – VI with Pu(III) and Pu(IV) dominant under reducing conditions, and even the oxidation states +II and +VII have been reported though not under environmentally relevant conditions. Americium is only stable as Am(III) in aqueous environments. Consequently, the chemical properties of the actinides in their trivalent state are fundamental for understanding their behavior in natural environments.

Glucuronic acid (GlcA) is a simple sugar acid, which is a common building block of extracellular polysaccharides (EPS), a ubiquitous biomolecule involved in numerous biochemical processes.[5-7] In aqueous solution it is typically present as a pyranoid six-ring in $^4C_1$ chair conformation, as a mixture of its two enantiomers α- and β-glucuronic acid. Their relative proportion varies in the literature, with some indication for a favorability of the β-form.[8, 9] A third isomer, γ-glucuronolactone, an intramolecular ester may become the preferred form at higher pH, but forms only very slowly.[10]

One important process affected by GlcA coordination is biomineralization, where EPS are presumed to be involved in metal transport processes.[7] Prior experiments in our group have shown that trivalent lanthanides (Ln), namely Eu(III), can be incorporated into minerals formed through a biologically-induced mechanism,[11] and it appears reasonable to assume the same process would prevail with An(III).[12, 13] A substitution of An(III) for Ca^{2+} in a biomineralization process, is also the

proposed mechanism for their incorporation into bone, which is mainly responsible for the long biological half-life of these elements.[14-16]

Some prior studies regarding the complexation behavior of GlcA with Ln(III)[17-21] and trivalent transition metals[22, 23] can be found in the literature. To our knowledge no studies of the complexation of An with GlcA exist to date. For the lanthanides, 1:1 and 1:2 complexes are reported, but evidence for the formation of the latter is only indirect. A number of different complex geometries have been suggested, which only agree on participation of the carboxyl group on C-6 in the metal bonding. The most common motive includes additional bonding through the ring oxygen O-5,[18, 19, 21] while some include additional bonding via OH-functions of GlcA.[18] Some studies also report stability constants, but none gives sufficient information for an extrapolation to standard conditions. The formation constants for the Ln:GlcA 1:1 complexes are in a range from $log\beta_{11}$ = 1.13 – 1.60[17, 24], those for the 1:2 complex range from $log\beta_{12}$ = 3.61 – 3.92.[17] For Cr(III) a 1:1 and 1:2 complex is described in the literature with lower complex formation constants ($log\beta_{11}$ = −0.13 and $log\beta_{12}$ = −2.24).[22]

We have studied the complex formation of GlcA with Cm(III) and Eu(III) as a representative of the trivalent actinides and a homologue, respectively. We made use of the excellent luminescence properties of both ions[25, 26] to apply time-resolved laser-induced luminescence spectroscopy (TRLFS) to determine the speciation of the ions in contact with GlcA, and to derive thermodynamic constants. Experiments at several ionic strength enabled the extrapolation of these parameters to infinite dilution, as well as derivation of a Specific Ion Interaction Theory (SIT) parameter $\varepsilon([Eu(GlcA)]^{2+};Cl^-)$ for Eu(III). From the complexes fluorescence lifetimes, the number of water molecules remaining in the ions' hydration sphere can be determined.[27-29] In combination with Nuclear Magnetic Resonance NMR spectroscopy and Density Functional Theory (DFT) calculations this allows for an unambiguous assignment of a complex structure.

2 Experimental

2.1 Sample preparation

Samples for Eu(III) luminescence experiments were prepared from stock solutions of NaCl (>99,5 %, p. a., Carl Roth GmbH& Co. KG, Germany), D-glucuronic acid (>97%, Fluka, Germany), and Eu(III) (from $EuCl_3 \cdot 6H_2O$, 99,9 %, Aldrich). The pH of all stock solutions was adjusted to pH = 5.0 with NaOH and HCl; the same were used for all other pH adjustments. All preparations (except for the series in the presence of CO_2) were performed in a glovebox with N_2 atmosphere. Three types of experiments were performed (s. Tab.1): 1. three series with variable ligand concentration at fixed pH = 5.0 and three ionic strengths, 2. One series with varying pH = 5 – 9 at lowest ionic strength, and 3. one ligand concentration series in the presence of CO_2.

Table 1: Experimental conditions for luminescence experiments.

Series	**I_m (mol kg^{-1}_{H2O})**	**[M(III)] (µmol/L)**	**[GlcA] (mmol/L)**	**pH**
Eu_I	0.0981	5.33	0.05 – 24.9	5.0
	0.455	5.33	0.50 – 49.9	5.0
	0.919	5.33	0.50 – 349	4.7[1]
Eu_pH	0.0981	5.32	0.50	5.0 – 9.0
Eu_CO_2	0.0094	4.94	0.05 – 47.5	8.3
Cm_I	0.0894	0.34	0.04 – 23.3	5.0

	0.911	0.34	0.14 – 66.0	4.7[1]

For the corresponding Cm(III) experiments a stock solution of ^{248}Cm ($t_{1/2}$ = 3.40 × 10^5 a) was used and all other steps were performed analogous to the Eu(III) experiments. Here, only two series with high and low ionic strength were performed as given in Table 1.

For the NMR experiments with Eu(III) and Y(III), 14.6mg $YCl_3 \cdot 6H_2O$ or 17.6 mg $EuCl_3 \cdot 6H_2O$ (0.048 mmol, >99.0 %, Merck KGaA and 99.9 %, Aldrich, respectively) and 9.8 mg D-glucuronic acid (0.050 mmol, >97 %, Fluka) were dissolved in 1mL D_2O (99.5 %, Deutero GmbH). The pD value was adjusted to 5.0 using NaOD and DCl (both 99.5 %, Deutero GmbH), assuming pD = pH*+0.4.

2.2 TRLFS experiments

All luminescence measurements were carried out in solution at room temperature. The samples were resonantly excited using a tunable OPO laser system (PANTHER EX OPO, Continuum, USA) pumped by a Nd:YAG laser (Powerlite Precision II 9020, Continuum, USA). Eu(III) was excited via its most intense absorption band corresponding to the ($^7F_0 \longrightarrow {}^5L_6$) transition at 394.0 nm, while the most intense ($^8S_{7/2} \longrightarrow {}^6I_{11/2}$) transition at 396.6 nm was used for Cm(III) excitation. Luminescence emission was collected using an optical fiber and transferred to an optical multi-channel analyzer (Oriel MS 257, United Kingdom) coupled with an Andor iStar (United Kingdom) iCCD detector. The detector was cooled to –20°C to reduce electronic noise. Generally, spectra were recorded with a delay after the laser pulse of 1 µs for a gate width of 10 ms. For time dependent measurements, the delay was increased over 60 steps of 5 – 25 µs each, according to the luminescence lifetime of the dominant species.

2.3 NMR experiments

NMR spectra were recorded on a Varian Inova 400 MHz spectrometer at 399.89 MHz for ^1H and 100.56 MHz for ^{13}C spectra, respectively. The D_2O solvent was used as the internal standard.

2.4 Quantum Mechanics/Molecular Modeling

Equilibrium Quantum Mechanics/Molecular Modeling (QMMM) simulations were conducted of each of Eu(III), Cm(III), and Y(III) with each of the α and β anomers of glucuronic acid where the metal was placed either above or below each anomer for a total of twelve configurations.

Production QMMM simulations were conducted with CHARMM 38b2 [30] and Turbomole 7.3.1 [31] for the `QM' subsystem via the CHARMM/Turbomole interface [32].

A cubic TIP3[33] water box with edge distance of 10Å was generated to ensure complete coverage of the complex molecule. Na^+ and Cl^- counter ions were added to a concentration of 150mM. Periodic boundary conditions were applied. For equilibration steps, a harmonic constraint of 24 kcal/mol/Å² was first applied. This was followed by short minimizations of 50 steps each (SD/Adopted Basis Newton-Raphson[34]) to relax the structure. An equilibration simulation of time step 1 fs was run for 250 ps at a temperature of 303.15 K. The Verlet integrator[35] and SHAKE algorithms[36] were used in concert with the Nose-Hoover thermostat[37] to ensure a constant temperature. Checks were conducted of pressure, temperature, etc. to ensure stability prior to production simulations.

The `QM' subsystem for each simulation contained the glucuronic acid molecule, the metal ion and all water molecules within 5Å of the equilibrium positions of both. The quantum chemical portion of the QMMM calculation was calculated via a DFT hybrid functional at the B3LYP [38-40]/def2-SVP (C, O, H)/def2-TZVP (Eu, Cm, Y)[41] level of theory. Point charge embedding was used to ensure that forces acting on the MM region by the QM region were included in the Hamiltonian evaluated as part of the DFT calculation. Resolution of the Identity[42] (RI) and multipole accelerated RI-J[43] approximations were used.

Production Langevin QMMM simulations were run with a time step of 1 fs with the scalar friction coefficient (FBETA) set to 8.0 to assist in more thorough exploration of conformational space. Each simulation was run in total for 40 ps.

QMMM free energies were calculated via umbrella sampling and post-processed with the Weighted Histogram Analysis Method [44, 45]. The calculation was divided amongst 41 and 17 x 1 ps sampling windows with respect to 2D (metal:carboxylate) and dihedral free energy calculations, respectively. A constraint of 100 kcal/(mol·Å²) was applied for conformations within each window and reduced to 50 kcal/(mol·Å²) at longer distances to ensure adequate sampling of phase space. 2D free energy calculations were conducted with the 2d_wham [46] program. Adequate sampling of the free energy profile was verified by plotting histograms of the quantity of interest in each window. Overlap of plotted histograms was taken as a proxy indicator of sufficient sampling within the phase space of the simulation to reconstruct free energy curves.

All representations of simulations and optimized structures were created with VMD v1.9.3[47]. All plots and analyses were compiled with R [48] and the Tidyverse [49] using color blind-friendly palettes for all plots.[50] LOcally EStimated Scatterplot (LOESS) smoothing[51] was applied to time-series plots with a smoothing parameter value, α, of 0.75.

3 Results

3.1 Luminescence spectroscopy

To determine the complex formation constants, luminescence spectra with increasing ligand concentration were measured at constant [M(III)] and pH = 5.0 ± 0.3†, at different, constant ionic strength. For Eu(III) three series were measured [I_m(NaCl) = 0.0981, 0.455, and 0.919 mol kg^{-1}_{H2O}] and two series for Cm(III) [I_m(NaCl) = 0.0894 and 0.911 mol kg^{-1}_{H2O}].

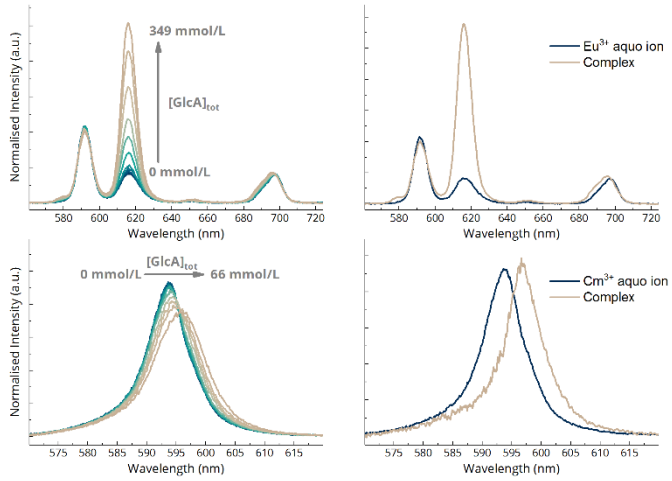

Figure 1: Luminescence spectra for Eu(III) (top, left) and Cm(III) (bottom, left) in the presence of GlcA at I_m(NaCl) = 0.919 and 0.911 mol kg^{-1}_{H2O}, respectively. The corresponding single component spectra obtained by peak deconvolution are shown on the right.

With increasing ligand concentration a continuous increase of the $(^5D_0 \longrightarrow {}^7F_2)/(^5D_0 \longrightarrow {}^7F_1)$ peak ratio is observed for Eu(III) (Figure 1) indicating a change in its coordination environment. In the case of Cm(III), the change in the coordination sphere results in a peak shift towards longer wavelength (Figure 1). These spectral changes must be related to a complexation reaction between Eu(III)/Cm(III) and GlcA.

The luminescence spectra can be used to derive the species distribution at each ligand-to-metal ratio. A peak deconvolution process via a least-squares fitting routine is applied to obtain pure component spectra and their relative contributions to the sum spectra, which must be corrected by each species' luminescence intensity (LI) factor to obtain the species distribution in solution. Detailed descriptions of the methodology are available in literature.[52] We find two components under all conditions for both Eu(III) and Cm(III). The pure component spectra are shown in Figure 1 on the right side (top: Eu, bottom: Cm). One component is the metal aquo ion and the other is tentatively assigned to an M-GlcA complex. The complexes have larger LI factors relative to the aquo ions of ~2.3 (Eu) and 1.3 (Cm), respectively. In one case, the sum spectrum could not be fully reproduced with these two species. At highest ionic strength (0.911 mol kg^{-1}_{H2O}) and highest ligand concentration (0.066 mol L^{-1}, Ligand/Metal (L/M) ratio ~ 2×10^5) the Cm(III) spectra show a residual after deconvolution (s. SI), which may be indicative of the formation of a second complex species. However, even at this large L/M ratio the species represents a very small fraction of the Cm(III) speciation and further characterization was not possible. Increasing ionic strength reduces the complex formation strength, i.e. higher ionic strengths require larger ligand concentration to produce the same amount of complex. Spectra at lower ionic strengths are available in the SI.

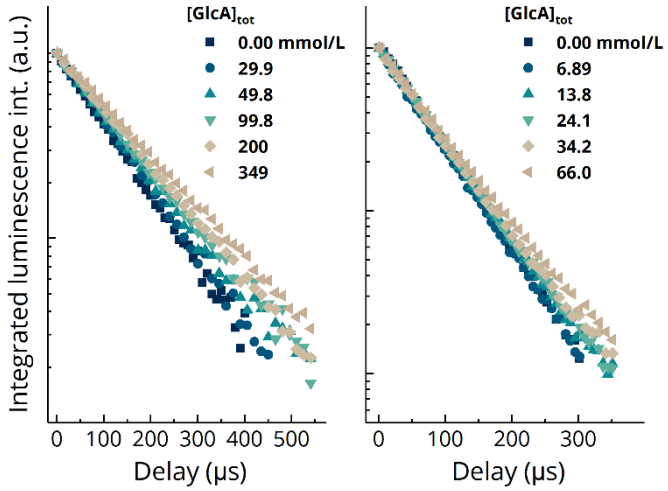

Figure 2: Luminescence decay profiles of Eu(III) (left) and Cm(III) (right) as a function of $[GlcA]_{tot}$ at I_m(NaCl) = 0.919 and 0.911 mol kg^{-1}_{H2O}, respectively.

With increasing ligand concentration, an increase in luminescence lifetime is observed for both ions (s. Figure 2). The luminescence lifetimes of both species were determined by an exponential fit of the luminescence decay profiles. For the M(III) aquo ions we find lifetimes of 114 ± 6 µs for Eu(III) and 69 ± 4 µs for Cm(III) in good agreement with literature values,[27-29] thus confirming the assumed initial speciation. The complex species has longer lifetimes in both cases. We find lifetimes of τ_{Eu} = 160 ± 13 µs and τ_{Cm} = 110 ± 10 µs, respectively. We can use eq. 1[27, 29] and 2[28, 29] to calculate the amount of water molecules N(H_2O) remaining in the ions' coordination spheres.

Eu: $$N(H_2O) = \frac{1.07\mu s}{\tau_{Eu}} - 0.62 \qquad (1)$$

Cm: $$N(H_2O) = \frac{0.65\mu s}{\tau_{Cm}} - 0.88 \qquad (2)$$

The calculation yields N(H_2O) = 6.1 ± 0.5 for Eu(III) and N(H_2O) = 5.0 ± 0.5 for Cm(III). The values agree reasonably well, indicating that GlcA has replaced 3 – 4 H_2O from the ions' coordination sphere. A limitation of this approach with respect to GlcA is that the ligand itself contains several OH-groups, which would be capable of vibrationally quenching Eu(III) and Cm(III) luminescence. If one or more OH-groups of GlcA bind directly to the metal centers, the number of coordinating water molecules could then be lower, accordingly.

3.2 Determination of complex formation constants and stoichiometry

The single component spectra and LI factors described above can be applied to determine the species distribution of Eu(III) and Cm(III) in the presence of GlcA. These distributions are shown in Figure 3. It must be noted once again that the Cm(III) speciation at highest [GlcA] is associated with a larger error due to the presence of the third uncharacterized species.

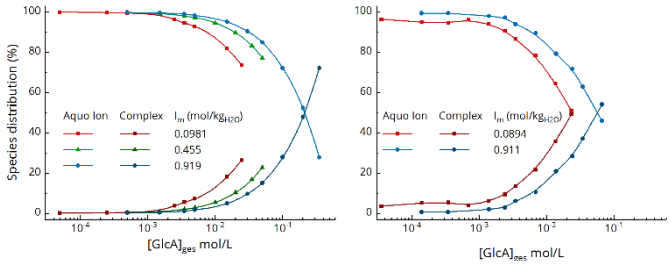

Figure 3: Speciation of Eu(III) (left) and Cm(III) (right) as a function of $[GlcA]_{tot}$ at various I_m determined from TRLFS. The relative contribution of the aquo ion is displayed in light colors, the GlcA-complex in dark colors. The lines are guides-to-the-eye.

In none of our experiments complete complexation was achieved, with the maximum at ~72% for Eu(III) at an L/M ratio ~ 6.6×10^4 with an ionic strength of 0.919 mol kg^{-1}$_{H2O}$ NaCl. Since the concentrations of Eu(III) and Cm(III) were orders of magnitude lower than that of GlcA, it is safe to assume that the equilibrium concentration of the acid was not significantly affected by the complexation reaction. By applying the law of mass action, the following expression of the conditional stability constant was obtained:

$$\log \beta = \log\left(\frac{[Eu(GlCA)_n]^{(3-n)+}}{[Eu_{aq}^{3+}]}\right) - n \cdot \log[GlcA] \quad (3)$$

$$\log\left(\frac{[Eu(GlCA)_n]^{(3-n)+}}{[Eu_{aq}^{3+}]}\right) = n \cdot \log[GlcA] + \log \beta \quad (4)$$

The linearized form, eq. 4, can now be used to obtain both, the stoichiometric parameter n and the conditional complex formation constant β. All results of the thermodynamic calculations are summarized in Table 2. The corresponding plots are shown in the SI. For Cm(III) some points at low [GlcA] deviate significantly from the slope obtained from the other data points. At these conditions, only small quantities (< 5%) of the complex have formed and the species distribution determination is strongly affected by small irregularities in the spectra. As such, these points were not considered for the determination of the complex formation constant. We also omitted the two last points of the Eu(III) series at highest I_m, due to the fact that the ligand concentration for these data points (0.200 and 0.349 mol L^{-1}, respectively) was sufficiently high to contribute considerably to the ionic strength. It should be noted however, that consideration of these data does not significantly change the calculated complex formation constant.

Table 2: Results from slope analysis for the determination of log β and stoichiometry.

	I_m (mol kg^{-1}$_{H2O}$)	**Slope *n***	***log*β**	***log*β* [1]**	**R^2**
Eu(III)	0.0981	0.97	1.11	1.19	0.99/0.99
	0.455	0.95	0.68	0.79	1.00/1.00
	0.919	1.05	0.70	0.58	0.99/1.00
Cm(III)	0.0894	0.91	1.44	1.66	0.99/0.98
	0.911	1.02	1.26	1.23	0.99/0.99

[1]log β^* denotes values determined by slope analysis with *n* fixed at 1. The same values were obtained from the species distribution (see SI).

The slopes for all series are consistently close to 1, indicating that the formed complex is $[M(GlcA)]^{2+}$ in all cases. There is no indication for the formation of the 1:2 complex postulated in the literature, with the exception of the single data point at L/M ~ 2.0×10^5 for Cm(III), and we conclude that this species would only form under extreme conditions. The conditional *log*β values, corresponding to the intercept at origin of the linear fits, are small for both cations, and show the expected decreasing trend for higher ionic strengths. As the fitted values of *n* are all equal to 1, within error of the method, data were refit with *n* fixed to 1.00, thus making the intercept *log*β the only free parameter. The quality-of-fit is not affected by this approach for any of the experimental series. Alternatively, the conditional *log*β can be calculated from the speciation at each L/M ratio (see SI). Under the omission of the same outliers as described for the slope analysis, and using the 1:1 stoichiometry obtained from it, we find the same conditional complex formation constants by this approach as by slope analysis with *n* fixed to 1.00.

3.3 Extrapolation of *log*β to infinite dilution

The extrapolation of the conditional complex formation constants was calculated using SIT.[53] Briefly, the activity coefficient of a species j is expressed as:

$$log\gamma_j = -z_j^2 D + \sum_k \varepsilon(j;k) m_k \qquad (5)$$

with z_j being the charge of the species, ε(j;k) the ion interaction parameters, m_k the molality of species k, and D the Debye-Hückel term:

$$D = \frac{A\sqrt{I_m}}{1+Ba_i\sqrt{I_m}} \quad (6)$$

where A is the Debye-Hückel constant (A = 0.509 $kg^{1/2}$ $mol^{-1/2}$ at 25°C[53]) and Ba_i = 1.5 $kg^{1/2}$ $mol^{-1/2}$ for all temperatures < 80°C.[53] The complex formation constant at zero ionic strength $log\beta^0$ and the conditional constant *log*β are then related by eq. 7:

$$log\beta - \Delta z^2 D = log\beta^0 - \Delta\varepsilon I_m (7)$$

with Δε defined as:

$$\Delta\varepsilon = \varepsilon(MGlcA^{2+}; Cl^-) - \varepsilon(M^{3+}; Cl^-) - \varepsilon(Na^+; GlcA^-). \qquad (8)$$

We can use analogous values from literature for two of these interaction parameters. For $\varepsilon(M^{3+}; Cl^-)$, we use the parameter $\varepsilon(Nd^{3+}; Cl^-) = 0.23 \pm 0.02\ kg_{H2O}mol^{-1}$, which is the recommended value in the NEA TDB.[53] The only interaction parameter for $GlcA^-$ accessible from literature data is $\varepsilon(K^+; GlcA^-) = -0.07\ kg_{H2O}mol^{-1}$ (see SI for determination of this parameter). We can now plot $log\beta - \Delta z^2 D$ with $\Delta z^2 = -6$ as a function of I_m and apply a linear regression to determine $log\beta^0$ and Δε (see SI). The derived parameters for Eu(III) are $log\beta^0$(Eu) = 1.84 ± 0.22 and Δε = –0.068, which gives $\varepsilon(EuGlcA^{2+}; Cl^-) = 0.24 \pm 0.36\ kg_{H2O}mol^{-1}$based on the values listed

above. For Cm(III) only two ionic strengths were considered. As it is not useful to perform a linear regression through only two points, we instead assume that the interaction parameters for similar ions will be similar[53], and set $\varepsilon(CmGlcA^{2+}; Cl^{-}) = \varepsilon(EuGlcA^{2+}; Cl^{-})$. The thus obtained standard complex formation constant is $log\beta^0$(Cm) = 2.39 ± 0.19.

3.4 Complex formation as function of pH

To evaluate the influence of pH on the complex formation we compare Eu(III) luminescence over the pH range from 5.0 to 9.0 in the presence and absence of GlcA. We chose solution conditions where complex formation is negligible (~ 1%) at pH = 5.0: [Eu] = 5.3 × 10^{-6} mol L^{-1}, [GlcA] = 5.0 × 10^{-4} mol L^{-1}, I_m = 0.09 mol kg^{-1}_{H2O}. The comparative approach is required to discern hydrolysis and complex formation in a straightforward manner. Emission spectra clearly show an effect of complex formation on Eu(III) speciation (see SI). It becomes most obvious, when observing the $^7F_2/^7F_1$ band intensity ratio, which is unaffected by pH up to value of ~7.5 with and without ligand, but increases strongly in the presence of GlcA at higher pH values, indicating a change in Eu(III)'s ligand field. In the absence of the ligand, a comparable increase occurs only at higher pH > 8.

Clearly, this change in coordination at pH = 7.5 is related to a complexation reaction, as it only occurs in the presence of the ligand. However, pH dependent changes of GlcA speciation are not expected in this range, as the carboxylic acid, with a pK_a of 3.3 should be fully deprotonated at much lower pH. A second pK_a = 12.2 can be found in the literature, but was not assigned to a specific deprotonation reaction in the molecule.[20] Considering the structure of the sugar acid, it must be related to the deprotonation of one of the OH-groups. The acidity of these OH-groups would be expected to increase upon coordination by a metal cation. For instance, Ferrari and co-workers reported deprotonation of an OH-group coordinated to Hg(II) already at pH > 7.[54] Consequently, we suggest that an OH-group coordinated to Eu(III) becomes deprotonated at pH > 7.5, leading to the formation of a more stable complex.

At yet higher pH > 9, the $^7F_2/^7F_1$ band intensity ratio once again is identical in the presence and absence of the ligand, indicating that later hydrolysis species suppress the formation of any Eu-GlcA complexes. The same is observed in the presence of atmospheric CO_2 at pH = 8.3 (calcite buffer pH), where identical emission spectra and $^7F_2/^7F_1$ band intensity ratios are measured up to a ligand concentration [GlcA] = 4.75 × 10^{-2} mol L^{-1} (L/M ≈ 9600). (see SI)

3.5 Structure of GlcA complexes

Beyond the thermodynamic description, it is important to understand the structure and bonding situation of the formed complex. Several aspects can be directly derived from the luminescence data discussed above. The complex has a 1:1 stoichiometry and we see only weak evidence for the formation of a 1:2 complex at very high L/M ratios. Lifetime measurements indicate that Eu(III) and Cm(III) luminescence is quenched by 5 – 6 water molecules in their first coordination sphere, also in agreement with the 1:1 stoichiometry. The luminescence data is, however, not suited to delineate which functional groups of the ligand are used in bonding to the cations. Here, a combination of NMR spectroscopy and QMMM calculations was used to derive the complex geometry.

Direct information about metal bonding in the complex can be derived from paramagnetic shifts in ^{13}C NMR. Comparison of chemical shifts in the free ligand, an isostructural complex with a diamagnetic cation, and the complex with the paramagnetic Eu(III) ion allows for the discrimination of paramagnetic effects through bonds and through the solvent. Thus, an assignment of the ligand's functional group involved in complex formation is possible. Chemical shifts for the free ligand are available in the literature.[19, 55] We chose Y(III) as a diamagnetic reference for Eu(III), with the expectation that both trivalent rare earth cations would form the same complex.

NMR shifts relative to free GlcA in D_2O at pD 5.0 for the ligand in contact with Y(III), and the free and complexed ligand in contact with Eu(III) are summarized in Table 3. The spectra of GlcA in contact with Y(III) show only weak signals for two different complex species. Both have signals at

around 5 ppm indicating, that only α-anomers are involved in the observed complexes. Coupling constants of adjacent ring protons indicate that the expected boat configuration of GlcA (all coupling constants expected to be between 3-5 Hz[56]) is distorted ($^3J_{(H\text{-}1,H\text{-}2)}$ = 4,5 Hz, $^3J_{(H\text{-}2,H\text{-}3)}$ = 7,4 Hz, ^3J = 7,4 Hz, $^3J_{(H\text{-}4,H\text{-}5)}$ = 3,2 Hz) enabling the hydroxyl groups 2 and 4 to be in an axial position and thus being able to complex Y on the bottom side of the sugar molecule. Consequently, the biggest shift deviations compared to the free ligand are found for C-2 and C-4, indicating bonding to the corresponding OH-groups. It is noteworthy that the carboxylic C-6 shows the smallest shift of all carbons (0.7 ppm) which would indicate no binding to C-6 occurs. This is however relative to the undistorted anomers, which may influence the interpretation.

Table 3: Metal induced ^{1}H and ^{13}C NMR-chemical shifts of GlcA in contact with Y(III) and Eu(III). Shift values are relative to free ligand in absence of metal ions under similar conditions.

	Y(III) / ppm		Eu(III) / ppm		
Atom	**complex 1**	**complex 2**	**free α-GlcA**	**free β-GlcA**	**complex**
H-1	0.14	−0.01	0.82	−0.16	1.89
H-2	0.65	0.54	0.27	−0.08	6.70
H-3	0.75	0.65	−0.65	−0.43	0.26
H-4	1.13	1.07	−0.26	−0.11	−0.15
H-5	0.51	— [a]	−0.69	−0.65	−6.89
C-1	2.5	— [a]	0.8	−0.4	4.1
C-2	4.6	— [a]	0.0	−0.2	9.8
C-3	2.0	— [a]	−0.2	−3.1	7.5
C-4	6.0	— [a]	0.2	2.6	0.2
C-5	2.4	— [a]	−20.3	−20.7	−9.0
C-6	0.7	— [a]	— [a]	— [a]	— [a]

[a] not observed

In contact with Eu(III) paramagnetic effects of the metal center may be propagated through solution (resulting in a net shift of all solvent accessible nuclei) as well as through dipolar interactions occurring only close to the metal center (pseudo contact shifts – PCS). This solvent propagated paramagnetic shift is consistently observed in the free ligand's signals of the α- and β- GlcA. The complex species of GlcA with Eu(III) shows large shifts relative to the free ligand for protons H-2 ($\Delta\delta = 6.70$ ppm) and H-5 ($\Delta\delta = -6.89$ ppm). The opposite relative shift directions indicate that those protons are located in two different orientations of the PCS cone of Eu(III)[57] and thus are in two different regions relative to the principal magnetic axis (perpendicular to and in the direction of the principal magnetic axis, respectively). The absolute value of these two relative shifts suggests that both protons are rather close to the metal center as would be the case in structure B in Figure 4, where the β-anomer of GlcA is in a conformation closest to the canonical $B_{1,4}$ but skewed towards $^3S_1$ and with a large puckering parameter Q (Cremer-Pople parameters: Φ = 55.124°, θ = 86.674°, and Q = 0.796 Å).[58] This is reflected in the relative shifts of the carbons as well with C-1, C-2, and C-3 located in the same cone part (closer to the direction of the principal magnetic axis), C-4 with close to no additional chemical shift located in the transition region around 55° and C-5 again being situated in the perpendicular region. A signal of the carboxylic carbon C-6 cannot be observed in our spectra despite a broad scanning range. In other publications C-6 was found to have a large positive shift if complexation occurs with O-6 and O-5.[19, 59] However, this would indicate that C-6 should

again be situated close to the direction of the principal magnetic axis like C-1, C-2 and C-3 and would require Eu(III) to insert deeply into the ring structure. The orientation of the principal magnetic axis is strongly dependent of the experimental conditions and the other complexing molecules and thus may vary according the conditions used. Overall, our experimental results suggest bonding of Eu(III) through one or two OH-groups, the ring oxygen O-5 as well as possibly the carboxylic acid group on C-6. Y(III) On the other hand, appears to bind to O-2 and O-4 of a distorted GlcA molecule. Obviously, the assumption of isostructural Y and Eu complexes was not valid, which means Y(III) cannot serve as a diamagnetic reference compound. A more detailed structural analysis is possible based on quantum chemical calculations, which are described in detail below.

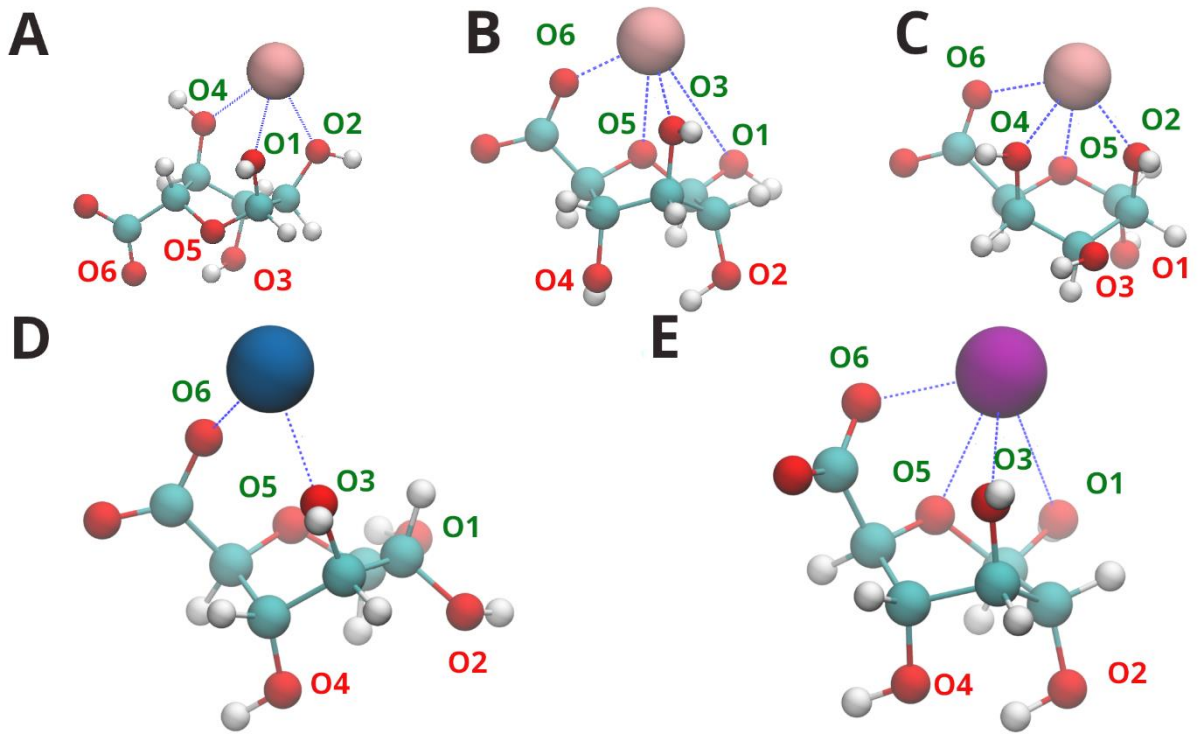

Figure 4: Depiction of Y(III) simulation starting geometries with (A) α -glucuronic acid (B) β -glucuronic acid and (C) the underside of a distorted α -glucuronic acid conformation. The most stable configurations from the QMMM simulations for (D) Eu and (E) Cm are shown below.

3.6 Computational analysis

We applied QMMM simulations to evaluate the stability of M(III) binding to either anomer of GlcA, as well as both sides of the ring of either anomer. These simulations can give insight into the apparent different coordination environment observed for Eu(III) and Y(III) in NMR and give an indication for the origin of the differences in stability observed for Eu(III) and Cm(III) by TRLFS. A total of twelve simulations was performed with Eu(III), Cm(III), and Y(III) in contact with the α- and β-anomers of GlcA from either above or below.

We first evaluate bonding of Eu(III) and Cm(III) to the two anomers of GlcA. With respect to the α-anomer, stable complexes were predicted for both Eu(III) and Cm(III) when the metal was placed over the ring and neither metal retrieved a stable complex when placed below the ring. However, binding to the top side was reliant upon the formation of a charged interaction between the metal ion and one of the ring hydroxyls after a deprotonation event, something only observed experimentally at pH values > 7.5. As most luminescence and NMR data were collected at lower pH values, binding to either side of the α-anomer was discounted for both Eu(III) and Cm(III).

Eu(III) was predicted to form interactions with either side of β-GlcA. Binding to the top includes an ionic interaction with glucuronic acid's terminal carboxylate. Thus, the β-anomer in the over geometry would generally be considered the more likely geometry with stable interactions (Figure

5A). However, the non-covalent bonds predicted between Eu(III) and its interaction partners in both cases fluctuate and whilst the β-anomer in the over position would be assumed to form a stronger complex, it appears likely that there is some degree of Eu(III) binding to either of the over and under sides of β-GlcA. This becomes most obvious in the ring dihedral angle in the Eu(III) complex (Figure 5B), which changes as Eu(III)'s interaction with the GlcA ring oxygen (O-5) breaks, leading to a net instability in the complex. By comparison, interactions between Cm(III) and the top side of the β-anomer were substantially more stable than those with the underside. Stable non-covalent interactions were formed with one hydroxyl (O-3), the ring oxygen (O-5) and an ionic interaction with the carboxylate (O-6). These interactions formed and persisted through the entire simulation, while the dihedral angle remains nearly constant at ~45° (Figure 5D, E).

The difference in the stability between Eu(III) and Cm(III) with GlcA could then be traced back to the persistence of non-covalent interactions. While Cm(III) consistently binds to O-3, O-5, and O-6, Eu(III) only maintains contact to the carboxyl O6. The interaction with the ring oxygen O-5 broke concurrently with a change in the C1-C2-C3-C4 dihedral angle of the ring (Figure 5A, B), which eventually leads to a break between Eu(III) and the O-3 hydroxyl and further destabilization of the complex. The NMR investigations suggest Eu(III) binding to O-3, O-5, and most likely O-6. As NMR measures on a much longer time scale than our simulations, the results from both methods are in general agreement in so far as we can assume Eu(III) bound to O-6 will likely periodically attach and detach from O-3 and O-5 eventually leading to the interaction “on average” we observe by NMR. It appears that the complex observed on the NMR time scale is the most stable complex predicted by QMMM with bonding to O-3, O-5, and O-6 on the top side of the β-anomer.

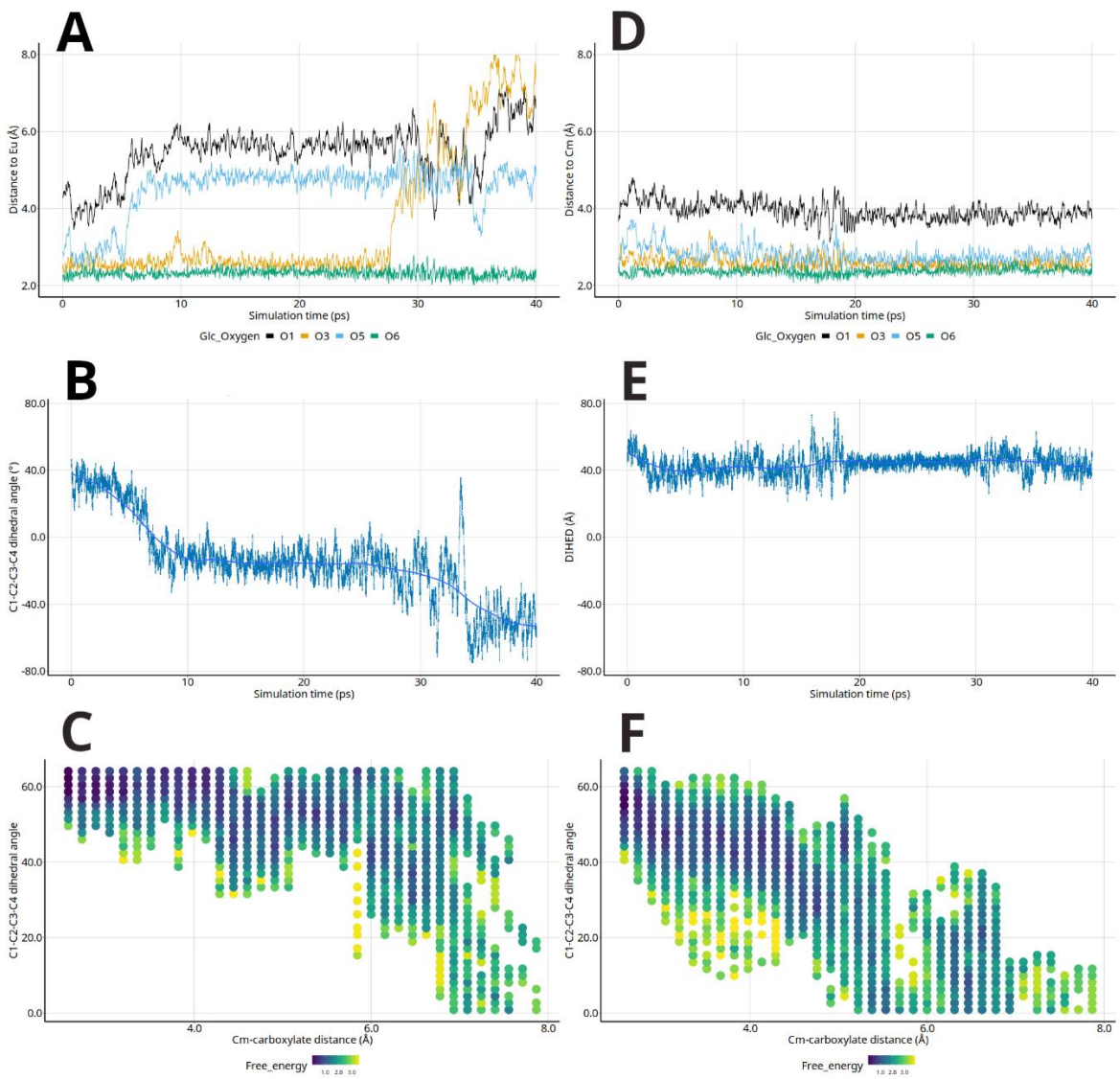

Figure 5: Stability comparison for β-GlcA complexes with Eu **(A-C)** and Cm **(D-F)** depicting the time evolution of bond distances between each metal with β-anomer oxygens (O-1, O-3, O-5, and acid carboxylate O-6), time evolution of a ring dihedral angle (C1-C2-C3-C4) and 2D free energy profile of each complex with respect to the metal:carboxylate bond and the ring dihedral angle.

To corroborate this interpretation, umbrella sampling simulations were conducted where interactions between the metal and interaction partners were constrained and free energy changes tracked in a reaction coordinate where the metal was placed at distances progressively away from the ring. These simulations were conducted in order to provide a comparison of the complex stability of Eu(III) and Cm(III) as a function of distance and the C1-C2-C3-C4 dihedral angle in the β-anomer ring. The more stable dihedral angle of ~45° from equilibrium simulations was observed with Cm(III) when the metal was within hydrogen bonding distances. Consequently, the calculated free energy for Cm(III) was lowest within these boundaries (Figure 5F). At the same distances, there was an increase in the C1-C2-C3-C4 dihedral angle to ~60° for Eu(III) and this was interpreted to mean that positioning of Eu(III) within these distances induces considerable ring strain to maintain all interactions with the β-anomer, which is only relieved at distances where Eu(III) is predicted to dissociate from ring interaction partners (Figure 5C). This is indicative of the greater stability of the complex with Cm(III).

We used the same approach to rationalize the unusual binding mode of Y(III) observed by NMR spectroscopy. In support of the experimental findings, our simulations yielded no stable binding geometries of Y(III) with the α- or β-anomer, above or below the pyranoid ring (see SI, Figure S12).

Similar to the findings for Eu(III) a C1-C2-C3-C4 dihedral angle of ~60° indicates significant ring strain induced by the non-covalent interactions between Y(III) and ring hydroxyls. This strain can only be alleviated by breaking at least one of the interactions. Stable bonding of Y(III) to GlcA can be achieved through a distortion of the α-anomer (see Figure 4C): a twist of the carboxyl group from below to above the ring, allows Y(III) simultaneous access to interaction partners otherwise only accessible in the α- (O-2 and O-4) or the β-anomer (O-5 and O-6) (Figure 4A-C). In this conformation interaction with Y(III) and the dihedral angle are predicted to be stable, indicative of a stable complex persisting for the duration of the simulation (Figure 6A and B). NMR suggests bonding only occurs to O-2 and O-4 and especially C-6 (indicative of bonding to O-6) shows only a very small shift. However, this is of course based on the comparison to the default conformation of the α-anomer and the peak position for C-6 will depend on the conformation to a certain degree, e.g. its signals in the α- and the β-anomer are shifted by 1.0 ppm. Altogether, our experimental findings cannot confirm or disprove the optimized structure from QMMM.

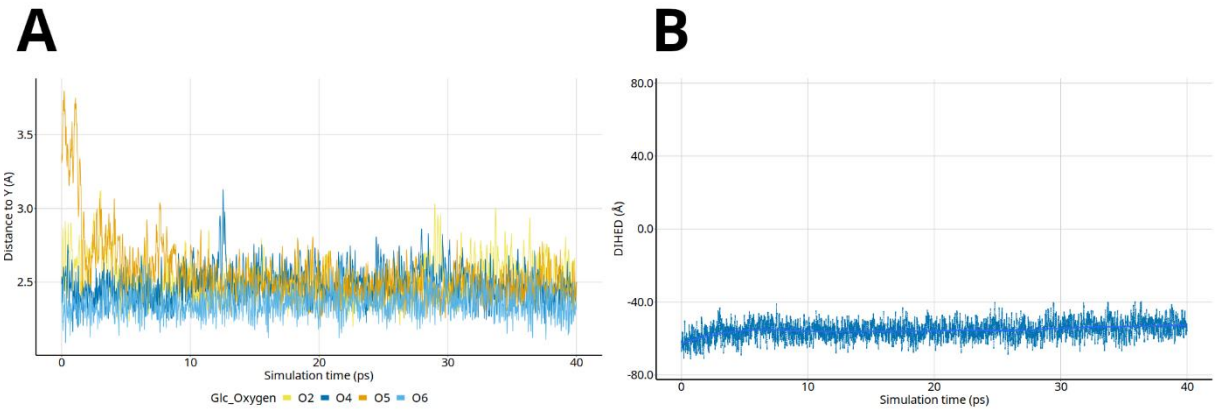

Figure 6: Time evolution of (A) bonds and (B) C1-C2-C3-C4 dihedral angle of simulation with Y(III) and the underside of α-glucuronic acid.

To assess the likelihood that the α-anomer could adopt this conformation, umbrella sampling simulations were conducted of both the free anomer and the distorted metal-bound conformation. For the free anomer, the C1-C2-C3-C4 dihedral angle was varied from the value when unbound to that observed in the metal-bound state (50° ⟶ −50°). For the metal-bound configuration, the opposite direction was modelled where the C1-C2-C3-C4 dihedral was varied from the metal-bound value to that observed in the unbound state (−50° ⟶ 50°). Free energy plots and diagnostic histograms for each sampling window can be found in the Supporting Information (Figure S11 and S12). It was determined that whilst there is a small free energy difference between the bound and unbound conformation (1.5 kcal/mol), the difference in the free energy for the opposite process was substantially greater at 245.5 kcal/mol (Figures S23 and S24, Supporting Information). The relatively small free energy difference between free α-anomer conformations is lower than that observed for flexible molecules such as cyclohexane[60] and suggests that both, the free anomer is able to easily interconvert between conformers in solution and that adoption of the twisted conformation occurs prior to stable metal binding. Further, these simulations suggest that upon complexation with Y(III), substantial stability is conferred.

4 Discussion

We have studied the complex formation of trivalent metals with glucuronic acid by experimental and quantum chemical means. We were able to determine the thermodynamic stability of the 1:1 complexes with Eu(III) and Cm(III) by TRLFS. We were able to determine complex formation constants $log\beta^0$ for both systems as well as ion interaction parameters for the Eu complex. Moreover, we could elucidate the likely structure and bonding in the complexes by a combination of TRLFS, NMR, and QMMM simulations.

4.1 Thermodynamic stability

The stability constants at infinite dilution determined by slope analysis of the TRLFS data indicate the formation of complexes of moderate strength, with $log\beta^0$(Eu) = 1.84 ± 0.22 and Cm(III) $log\beta^0$(Cm) = 2.39 ± 0.19. For various lanthanides complex formation constants between 1.13[17] and 1.60[20] had previously been determined in reasonable agreement with the value for Eu(III) determined here. The previous values had been determined at fixed ionic strength of either 0.1 or 1.0 mol/L, thus not allowing extrapolation to infinite dilution.

The values determined for Eu(III) ($log\beta^0$(Eu) = 1.84 ± 0.22) and Cm(III) ($log\beta^0$(Cm) = 2.39 ± 0.19) are significantly different, indicating a ~3.5× higher stability of the Cm(III) complex. While such behavior is not unusual *per se*,[61] it is not expected for a relatively weak ligand binding exclusively through oxygen donors. For instance, for citric acid[62] as a common organic acid and *N*-acetyl-neuraminic acid[63], which has a similar structure to uronic acids, the complex formation constants of Eu(III) and Cm(III) are identical within the respective error margins. A similar difference in complex formation, albeit with the higher stability for the Eu(III) complex was recently observed for $H_2PO_4^-$.[64] For the GlcA system we can speculate that the size difference between Eu(III) and Cm(III) is ultimately responsible for the differences in stability, which is corroborated by QMMM simulations (see below).

Both complexes are more stable than the corresponding Ca^{2+} complex, for which a $log\beta^0$(Ca) of 1.00 ± 0.11[9] and 1.50[65] has been reported. Were GlcA (e.g. as part of EPS) to act as Ca^{2+} transporter for e.g. biomineralization processes[7], Eu(III) and especially Cm(III) could replace Ca^{2+} in its complexes and thus be incorporated in the biogenic material. The results in the presence of ambient CO_2 show that the cations would be released in the presence of CO_3^{2-}, as would be expected based on the much higher stability of the metals' CO_3^{2-} complexes.

4.2 Structures

In addition to the thermodynamic investigations we were also able to characterize the structure of the formed complexes. In all cases 1:1 complexes with a "half sandwich" structure have been observed, as clearly indicated by the presence of ~5 water molecules in the first hydration shell of Eu(III) and Cm(III). Formation of a different complex species could only be observed at very large L/M ratios (~ 2 × 10^5). This species was only present in small quantities even at such large excess of GlcA and could thus not be characterized further. It is possible that this third species is indeed the 1:2 "sandwich" complex postulated previously [18, 21, 22], but an unambiguous identification is not possible.

Our results indicate differences in binding between all three investigated metal cations, most likely related to their different ionic radii [r_{ion}^{VI} = 97 (Cm); 94.7 (Eu), and 90 pm(Y)][66]. In the case of Cm(III), the QMMM simulations predict stable binding to O-3, O-5, and O-6 of the top side of β-GlcA. A similar binding motif had been observed for the relatively large La(III) cation (r_{ion}^{VI} = 103.2 pm) [18]. Our NMR results suggest that the time-averaged binding motif is the same for Eu(III). However, the QMMM simulations show that while this type of complex can indeed form, it is only stable for a limited time. The instability is linked to an unsuitable C1-C2-C3-C4 dihedral angle, which causes strain in the pyranoid ring and ultimately leads to breakage of Eu–O bonds. It appears that the small difference in ionic radii between Cm(III) and Eu(III) (Δr_{ion}^{VI} = 2.3 pm) causes sufficient strain in the GlcA ring backbone to affect the stability of the complex. The same ring strain must then also be responsible for the observed differences in stability between the two complexes. We observed a change in the complexation of Eu(III) at pH > 7.5, which is most likely related to a deprotonation reaction. As the carboxylic group is fully deprotonated at much lower pH, this would suggest a deprotonation of the coordinated OH-group, here OH-3. In its uncomplexed state, GlcA has a second pK_a ~ 12.04 ± 0.03 [20], more than four pH units higher than for the deprotonation reaction observed here.

The ring strain responsible for the destabilization of the Eu(III) complex should be yet more pronounced in the case of the smaller Y(III) cation. This is confirmed by both, NMR and QMMM, which unanimously show that the complex observed for Cm(III) with binding to O-3, O-5, and O-6 cannot form with Y. NMR finds binding most likely to O-2 and O-4 of the α-anomer, while QMMM simulations do not converge on any stable complex with either side of either anomer. The simulations only converge to a stable complex upon distortion of the molecule in such a way that binding to O-2 and O-4, the ring oxygen O-5, and the carboxylic O-6 becomes possible. This is in agreement with our observation from NMR spectroscopy that GlcA in the Y(III) complex is distorted from its nominal boat shape, but NMR did not detect binding to O-5 or O-6. Such a complex with a distorted GlcA had not been observed before. There is, however, evidence in the literature that smaller cation cannot form as stable complexes with GlcA. Fuks and Bünzli found a trend towards smaller complex formation constants for smaller lanthanide cations (i.e. Gd and Lu).[17] Balt et al. postulated a 1:2 complex for Yb(III) with GlcA in which both ligands bind only through O-5 and O-6 without any participation of the rings hydroxyl groups.

5 Conclusions

Glucuronic acid forms moderately strong complexes with Eu(III) and Cm(III) at mildly acidic pH, and the complex formation constant for Cm(III) ($log\beta^0$(Cm) = 2.39 ± 0.19) is slightly larger than that for Eu(III) ($log\beta^0$(Eu) = 1.84 ± 0.22). The origin for this difference in stability can be traced back to differences in ring strain due to the smaller size of Eu(III). At mildly alkaline pH (> 7.5) an apparently more stable complex is formed, most likely related to the deprotonation of a coordinated OH-group. At yet higher pH (> 9) GlcA complexes are, however, completely suppressed by hydrolysis and CO_3^{2-} complexation at pH values higher than 9.0.

The structure and stability of the GlcA complexes strongly depends on the size of the cations, which is related to strain in the pyranose ring, required to realise the three-fold coordination by the carboxylic group, ring-O-5, and an additional OH-group of β-GlcA. This coordination geometry is stable for the largest investigated ion Cm(III), but can only be temporarily realized for Eu(III), which leads to a reduced stability of the $[Eu(GlcA]^{2+}$ complex. For the smallest investigated cation Y(III), this leads to the formation of an entirely different complex, wherein the cation is coordinated by a distorted conformation of α-GlcA, while a stable interaction with the undistorted conformers could not be realized in QMMM simulations.

The GlcA complexes of both M(III) are stronger than the corresponding Ca(II) complex, which leaves the possibility for the substitution of Ca(II) by Cm(III) and other trivalent actinides or Eu(III) in biological processes. If GlcA containing EPS are involved in cation transport for biomineralization, such a substitution could lead to the incorporation of M(III) heavy metals into the newly formed material.

Conflicts of interest

There are no conflicts to declare.

Acknowledgements

This study was partially funded by the Helmholtz Association by funding the Helmholtz Young Investigator Group "Structures and reactivity at the aqueous/mineral interface" (VH-NG-942) and the German Federal Ministry of Education and Research (BMBF) under the project number 02NUK046B (FENABIUM).

Notes and references

† All solutions were set to a pH = 5.00 ± 0.05, but no ionic strength correction was considered for the highest ionic strength. As such, the actual pH will deviate from the measured pH by ~0.3 log units. As the speciation of Eu(III) and Cm(III) does not change in this pH range and deprotonation of GlcA is also constant the effect of pH deviations can be considered negligible.

Associated Content

Supporting Information available: TRLFS spectra at lower I; Residuals in Cm(III) TRLFS at highest I and highest [$GlcA^-$]; TRLFS spectra as a function of pH and in the presence of CO_2; Thermodynamic calculations; Additional QMMM results under equilibrium conditions; Results from QMMM umbrella sampling; ^1H NMR spectra.

(1) Geckeis, H.; Lützenkirchen, J.; Polly, R.; Rabung, T.; Schmidt, M., *Mineral–Water Interface Reactions of Actinides*, *Chem. Rev.* **2013,** *113*, 1016-1062.
(2) Gonzalez, E. *Physics and Safety of Transmutation Systems: A Status Report*; 6090; OECD-NEA: Paris, France, 2006; p 120.
(3) Kersting, A. B.; Efurd, D. W.; Finnegan, D. L.; Rokop, D. J.; Smith, D. K.; Thompson, J. L., *Migration of Plutonium in Ground Water at the Nevada Test Site*, *Nature* **1999,** *397*, 56-59.
(4) Novikov, A. P.; Kalmykov, S. N.; Utsunomiya, S.; Ewing, R. C.; Horreard, F.; Merkulov, A.; Clark, S. B.; Tkachev, V. V.; Myasoedov, B. F., *Colloid Transport of Plutonium in the Far-Field of the Mayak Production Association, Russia*, *Science* **2006,** *314*, 638-641.
(5) Dutton, G. J., *Glucuronic Acid: Free and Combined.* Academic Press: New York, 1966.
(6) Stout, B. E.; Deramos, C. M., *Interactions of Actinide Analogues with Naturally Occurring Organic Matter*, *MRS Proc.* **2011,** *353*, 197.
(7) Arias, J. L.; Fernandez, M. S., *Polysaccharides and Proteoglycans in Calcium Carbonate-Based Biomineralization*, *Chem. Rev.* **2008,** *108*, 4475-4482.
(8) Giner, J.-L.; Feng, J.; Kiemle, D. J., *Nmr Tube Degradation Method for Sugar Analysis of Glycosides*, *J. Nat. Prod.* **2016,** *79*, 2413-2417.
(9) Jaques, L. W.; Macaskill, J. B.; Weltner, W., *Electric Field Theory Applied to the Hydrogen-1 and Carbon-13 Nuclear Magnetic Resonance Spectra of Carbohydrates*, *J. Phys. Chem.* **1979,** *83*, 1412-1421.
(10) Blake, J. D.; Richards, G. N., *Problems of Lactonisation in the Analysis of Uronic Acids*, *Carbohydr. Res.* **1968,** *8*, 275-281.
(11) Johnstone, E. V.; Hofmann, S.; Cherkouk, A.; Schmidt, M., *Study of the Interaction of Eu^{3+} with Microbiologically Induced Calcium Carbonate Precipitates Using Trlfs*, *Env. Sci. Tech.* **2016,** *50*, 12411-12420.
(12) Schmidt, M.; Stumpf, T.; Walther, C.; Geckeis, H.; Fanghänel, T., *Phase Transformation in $Caco_3$ Polymorphs: A Spectroscopic, Microscopic and Diffraction Study*, *J. Colloid Int. Sci.* **2010,** *351*, 50-56.
(13) Schmidt, M.; Stumpf, T.; Marques Fernandes, M.; Walther, C.; Fanghänel, T., *Charge Compensation in Solid Solutions*, *Angew. Chem. Int. Ed.* **2008,** *47*, 5846-5850.

(14) Holliday, K.; Handley-Sidhu, S.; Dardenne, K.; Renshaw, J.; Macaskie, L.; Walther, C.; Stumpf, T., *A New Incorporation Mechanism for Trivalent Actinides into Bioapatite: A Trlfs and Exafs Study*, *Langmuir* **2012,** *28*, 3845-3851.
(15) Weiner, S., *Transient Precursor Strategy in Mineral Formation of Bone*, *Bone* **2006,** *39*, 431-433.
(16) Weiner, S.; Sagi, I.; Addadi, L., *Choosing the Crystallization Path Less Traveled*, *Science* **2005,** *309*, 1027-1028.
(17) Fuks, L.; Bünzli, J.-C. G., *Lanthanide-Ion Complexation by D-Glucuronic and D-Galacturonic Acids*, *Helvetica Chimica Acta* **1993,** *76*, 2992-3000.
(18) Fuks, L.; Filipiuk, D.; Lewandowski, W., *Lanthanide Ions Complexation by Uronic Acids*, *Journal of Molecular Structure* **2001,** *563–564*, 587-593.
(19) Izumi, K., *Carbon-13 NMR Spectra of Sodium D-Gluco- and D-Galacto-Pyranuronates in the Presence of Lanthanide Ions*, *Agricultural and Biological Chemistry* **1980,** *44*, 1623-1631.
(20) Makridou, C.; Cromer-Morin, M.; Scharff, J.-P., *Complexation De Quelques Ions Métalliques Par Les Acides Galacturonique Et Glucuronique*, *Societé Chimique* **1977,** *5*, 59-63.
(21) Balt, S.; de Bolster, M. W. G.; Visser-Luirink, G., *A 13c-N.M.R. Study of the Binding of Ytterbium(Iii) to Chondroitin Sulphate and Chondroitin*, *Carbohydr. Res.* **1983,** *121*, 1-11.
(22) Cetin, Z.; Kantar, C.; Alpaslan, M., *Interactions between Uronic Acids and Chromium(Iii)*, *Environmental Toxicology and Chemistry* **2009,** *28*, 1599-1608.
(23) Gyurcsik, B.; Nagy, L., *Carbohydrates as Ligands: Coordination Equilibria and Structure of the Metal Complexes*, *Coord. Chem. Rev.* **2000,** *203*, 81-149.
(24) Makridou, C.; Cromer-Morin, M.; Scharff, J. P., *Complexation De Quelques Ions Métalliques Par Les Acides Galacturonique Et Glucuronique*, *Bull. Soc. Chim. Fr.* **1977,** *5*, 59-63.
(25) Binnemans, K., *Interpretation of Europium(Iii) Spectra*, *Coordination Chemistry Reviews* **2015,** *295*, 1-45.
(26) Edelstein, N., *Optical and Magnetic Properties of Tetravalent Actinide Ions and Compounds*, *Journal of the Less Common Metals* **1987,** *133*, 39-51.
(27) Horrocks Jr., W. D.; Sudnick, D. R., *Time-Resolved Europium(Iii) Excitation Spectroscopy: A Luminescence Probe of Metal Ion Binding Sites.*, *Science* **1979,** *206*, 1194-1196.
(28) Kimura, T.; Choppin, G. R., *Luminescence Study on Determination of the Hydration Number of Cm(Iii)*, *Journal of Alloys and Compounds* **1994,** *213-14*, 313-317.
(29) Kimura, T.; Kato, Y.; Takeishi, H.; Choppin, G. R., *Comparative Study on the Hydration States of Cm(Iii) and Eu(Iii) in Solution and in Cation Exchange Resin*, *Journal of Alloys and Compounds* **1998,** *271-273*, 719-722.
(30) Huang, J.; Rauscher, S.; Nawrocki, G.; Ran, T.; Feig, M.; L de Groot, B.; Grubmller, H.; MacKerell, A. D., *Charmm36m: An Improved Force Field for Folded and Intrinsically Disordered Proteins*, *Nat. Methods* **2017,** *14*, 71-73.
(31) Gal, J.-Y.; Bollinger, J.-C.; Tolosa, H.; Gache, N., *Calcium Carbonate Solubility: A Reappraisal of Scale Formation and Inhibition*, *Talanta* **1996,** *43*, 1497-1509.
(32) Riahi, S.; Rowley, C. N., *The Charmm–Turbomole Interface for Efficient and Accurate Qm/Mm Molecular Dynamics, Free Energies, and Excited State Properties*, *J. Comput. Chem.* **2014,** *35*, 2076-2086.
(33) Jorgensen, W. L.; Chandrasekhar, J.; Madura, J. D.; Impey, R. W.; Klein, M. L., *Comparison of Simple Potential Functions for Simulating Liquid Water*, *J. Chem. Phys.* **1983,** *79*, 926-935.
(34) Chu, J. W.; Trout, B. L.; Brooks, B. R., *A Super-Linear Minimization Scheme for the Nudged Elastic Band Method*, *J. Chem. Phys.* **2003,** *119*, 12708-12717.
(35) Verlet, L., *Computer "Experiments" on Classical Fluids. I. Thermodynamical Properties of Lennard-Jones Molecules*, *Phys. Rev.* **1967,** *159*, 98-103.
(36) Ryckaert, J. P.; Ciccotti, G.; Berendsen, H. J. C., *Numerical Integration of the Cartesian Equations of Motion of a System with Constraints: Molecular Dynamics of N-Alkanes*, *J. Chem. Phys.* **1977,** *23*, 327-341.
(37) Hoover, W. G., *Canonical Dynamics: Equilibrium Phase-Space Distributions*, *Phys. Rev. A* **1985,** *31*, 1695-1697.
(38) Becke, A. D., *Density-Functional Thermochemistry. Iii. The Role of Exact Exchange*, *J. Chem. Phys.* **1993,** *98*, 5648-5652.

(39) Vosko, S. H.; Wilk, L.; Nusair, M., *Accurate Spin-Dependent Electron Liquid Correlation Energies for Local Spin Density Calculations: A Critical Analysis*, *Can. J. Phys.* **1980,** *58*, 1200-1211.
(40) Stephens, P. J.; Devlin, F. J.; Chabalowski, C. F.; Frisch, M. J., *Ab Initio Calculation of Vibrational Absorption and Circular Dichroism Spectra Using Density Functional Force Fields*, *J. Chem. Phys.* **1994,** *98*, 11623-11627.
(41) Weigend, F., *Accurate Coulomb-Fitting Basis Sets for H to Rn*, *Phys. Chem. Chem. Phys.* **2006,** *8*, 1057-1065.
(42) Eichkorn, K.; Treutler, O.; Öhm, H.; Häser, M.; Ahlrichs, R., *Auxiliary Basis Sets to Approximate Coulomb Potentials*, *Chem Phys Lett* **1995,** *240*, 283 - 290.
(43) Bauernschmitt, R.; Haser, M.; Treutler, O.; Ahlrichs, R., *Calculation of Excitation Energies within Time-Dependent Density Functional Theory Using Auxiliary Basis Set Expansions*, *Chem Phys Lett* **1997,** *264*, 573 - 578.
(44) Kumar, S.; Rosenberg, J. M.; Bouzida, D.; Swendsen, R. H.; Kollman, P. A., *Multidimensional Free-Energy Calculations Using the Weighted Histogram Analysis Method*, *J. Comput. Chem.* **1995,** *16*, 1339-1350.
(45) Roux, B., *The Calculation of the Potential of Mean Force Using Computer Simulations*, *Comput. Phys. Comm.* **1995,** *91*, 275-282.
(46) Grossfield, A., Wham: An Implementation of the Weighted Histogram Analysis Method. In.
(47) Humphrey, W.; Dalke, A.; Schulten, K., *{Vmd} -- {V}Isual {M}Olecular {D}Ynamics*, *J. Molec. Graph.* **1996,** *14*, 33-38.
(48) RCoreTeam *R: A Language and Environment for Statistical Computing*, 2013.
(49) Wickham, H.; Averick, M.; Bryan, J.; Chang, W.; McGowan, L.; François, R.; Grolemund, G.; Hayes, A.; Henry, L.; Hester, J.; Kuhn, M.; Pedersen, T.; Miller, E.; Bache, S.; Müller, K.; Ooms, J.; Robinson, D.; Seidel, D.; Spinu, V.; Takahashi, K.; Vaughan, D.; Wilke, C.; Woo, K.; Yutani, H., *Welcome to the Tidyverse*, *J. Open Source Softw.* **2019,** *4*, 1686.
(50) Goedhart, J. Material Related to the Blog "Dataviz with Flying Colors". http://doi.org/10.5281/zenodo.3381072
(51) Cleveland, W. S.; Devlin, S. J., *Locally Weighted Regression: An Approach to Regression Analysis by Local Fitting*, *J. Am. Stat. Assoc.* **1988,** *83*, 596-610.
(52) Huittinen, N.; Rabung, T.; Schnurr, A.; Hakanen, M.; Lehto, J.; Geckeis, H., *New Insight into Cm(Iii) Interaction with Kaolinite – Influence of Mineral Dissolution*, *Geochim. Cosmochim. Acta* **2012,** *99*, 100-109.
(53) Lemire, R. J.; Berner, U.; Musikas, C.; Palmer, D. A.; Taylor, P.; Tochiyama, O., *Chemical Thermodynamics of Iron Part 1*. OECD Publications: 2013; Vol. 13a.
(54) Ferrari, E.; Grandi, R.; Lazzari, S.; Saladini, M., *Hg(Ii)-Coordination by Sugar-Acids: Role of the Hydroxy Groups*, *J. Inorg. Biochem.* **2005,** *99*, 2381-2386.
(55) Gorin, P. A. J.; Mazurek, M., *Further Studies on the Assignment of Signals in 13c Magnetic Resonance Spectra of Aldoses and Derived Methyl Glycosides*, *Canadian Journal of Chemistry* **1975,** *53*, 1212-1223.
(56) Karplus, M., *Vicinal Proton Coupling in Nuclear Magnetic Resonance*, *J. Am. Chem. Soc.* **1963,** *85*, 2870-2871.
(57) Pintacuda, G.; John, M.; Su, X.-C.; Otting, G., *Nmr Structure Determination of Protein–Ligand Complexes by Lanthanide Labeling*, *Acc. Chem. Res.* **2007,** *40*, 206-212.
(58) Cremer, D.; Pople, J. A., *General Definition of Ring Puckering Coordinates*, *J. Am. Chem. Soc.* **1975,** *97*, 1354-1358.
(59) Angyal, S. J.; Greeves, D.; Littlemore, L., *The Structure of the Complex Formed from D-Galacturonate Ions and Cations in Solution*, *Carbohydr. Res.* **1988,** *174*, 121-131.
(60) Strauss, H. L.; Pickett, H. M., *Conformational Structure, Energy, and Inversion Rates of Cyclohexane and Some Related Oxanes*, *J. Am. Chem. Soc.* **1970,** *92*, 7281-7290.
(61) Adam, C.; Kaden, P.; Beele, B. B.; Mullich, U.; Trumm, S.; Geist, A.; Panak, P. J.; Denecke, M. A., *Evidence for Covalence in a N-Donor Complex of Americium(Iii)*, *Dalton Transactions* **2013,** *42*, 14068-14074.

(62) Heller, A.; Barkleit, A.; Foerstendorf, H.; Tsushima, S.; Heim, K.; Bernhard, G., *Curium(Iii) Citrate Speciation in Biological Systems: A Europium(Iii) Assisted Spectroscopic and Quantum Chemical Study*, *Dalton Transactions* **2012,** *41*, 13696-13983.
(63) Wilke, C. Spektroskopische Untersuchungen Zur Bindungsform Dreiwertiger Lanthanide Und Actinide in Biofluiden Des Menschlichen Verdauungssystems. TU Dresden, 2018.
(64) Jordan, N.; Demnitz, M.; Lösch, H.; Starke, S.; Brendler, V.; Huittinen, N., *Complexation of Trivalent Lanthanides (Eu) and Actinides (Cm) with Aqueous Phosphates at Elevated Temperatures*, *Inorg. Chem.* **2018,** *57*, 7015-7024.
(65) Gould, R. O.; Rankin, A. F., *Calcium Complexes of Uronic Acid Monomers*, *J. Chem. Soc. D* **1970**, 489-490.
(66) Shannon, R. D., *Revised Effective Ionic Radii and Systematic Studies of Interatomic Distances in Halides and Chalcogenides*, *Acta Crystallographica* **1976,** *A32*, 751-767.